

# Insights into $\text{TiO}_2$ thin film photodegradation from Kelvin Probe AFM maps

Cite as: Appl. Phys. Lett. **121**, 031901 (2022); <https://doi.org/10.1063/5.0098788>  
 Submitted: 12 May 2022 • Accepted: 29 June 2022 • Published Online: 20 July 2022

Tuza Olukan,  Jekaterina Sydorenko, Atanas Katerski, et al.



View Online



Export Citation



CrossMark

## ARTICLES YOU MAY BE INTERESTED IN

[Acoustic energy harvesting metasurface based on surface wave conversion](#)

Applied Physics Letters **121**, 031701 (2022); <https://doi.org/10.1063/5.0097676>

[Increasing the mobility and power-electronics figure of merit of AlGaN with atomically thin AlN/GaN digital-alloy superlattices](#)

Applied Physics Letters **121**, 032105 (2022); <https://doi.org/10.1063/5.0097963>

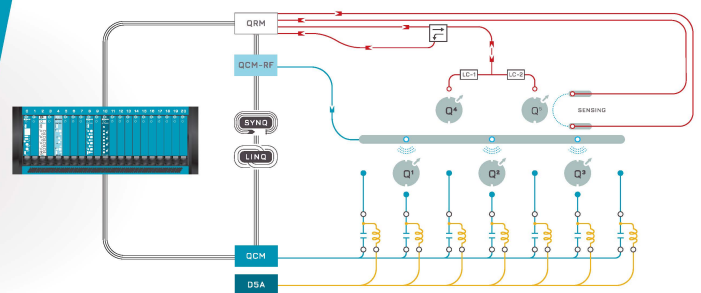
[50 °C low-temperature ALD  \$\text{SnO}\_2\$  driven by  \$\text{H}\_2\text{O}\_2\$  for efficient perovskite and perovskite/silicon tandem solar cells](#)

Applied Physics Letters **121**, 033502 (2022); <https://doi.org/10.1063/5.0091311>

 QBLOX

Integrates all  
Instrumentation + Software  
for Control and Readout of  
**Spin Qubits**

[visit our website >](#)



# Insights into TiO<sub>2</sub> thin film photodegradation from Kelvin Probe AFM maps

Cite as: Appl. Phys. Lett. **121**, 031901 (2022); doi: [10.1063/5.0098788](https://doi.org/10.1063/5.0098788)

Submitted: 12 May 2022 · Accepted: 29 June 2022 ·

Published Online: 20 July 2022



View Online



Export Citation



CrossMark

Tuza Olukan,<sup>1</sup> Jekaterina Sydorenko,<sup>2</sup>  Atanas Katerski,<sup>2</sup> Mariam Al Mahri,<sup>3</sup> Chia-Yun Lai,<sup>1</sup> Abdulrahman Al-Hagri,<sup>1,3</sup> Sergio Santos,<sup>1,a)</sup>  and Matteo Chiesa<sup>1,2,3,a)</sup> 

## AFFILIATIONS

<sup>1</sup>ARC-Arctic Centre for Sustainable Energy, Department of Physics and Technology, UiT The Arctic University of Norway, 9010 Tromsø, Norway

<sup>2</sup>Tallinn University of Technology, Department of Materials and Environmental Technology, Ehitajate tee 5, 19086 Tallinn, Estonia

<sup>3</sup>Laboratory for Energy and Nano Science, Masdar Campus, Khalifa University, Abu Dhabi, United Arab Emirates

<sup>a)</sup>Authors to whom correspondence should be addressed: [santos\\_en@yahoo.com](mailto:santos_en@yahoo.com) and [matteo.chiesa@uit.no](mailto:matteo.chiesa@uit.no)

## ABSTRACT

The synthesis of TiO<sub>2</sub> thin films by the chemical spray pyrolysis method at different titanium isopropoxide (TTIP) to acetylacetone (AcacH) ratios has been shown to lead to the highest photodegradation at 1 (TTIP):8 (AcacH). These films hold promise in the field of indoor pollution treatment. Carbon incorporation into the surface and into the TiO<sub>2</sub> lattice could be responsible for the observed performance, but the mechanism is still to be elucidated. Here, we report the correlation of contact potential difference (CPD) contrast maps as produced using Kelvin Probe Force Microscopy, and the observed functionality dependence on the TTIP to AcacH ratio. Since the CPD contrast locally provides information about the sample's Fermi level, this correlation provides a means to interpret enhanced photocatalytic activity in terms of the presence of acceptors that make possible a faster transfer of charge carriers to the surface.

© 2022 Author(s). All article content, except where otherwise noted, is licensed under a Creative Commons Attribution (CC BY) license (<http://creativecommons.org/licenses/by/4.0/>). <https://doi.org/10.1063/5.0098788>

The synthesis and optimization of TiO<sub>2</sub> thin films are rapidly advancing in fields such as environmental engineering, and has important and promising applications in the field of pollution treatment.<sup>1–3</sup> These applications rely on the principles of photocatalysis<sup>4,5</sup> and photoreactivity.<sup>6</sup> Applications could result in the reduction of outdoor/indoor pollution<sup>7</sup> without compromising the optimization of thermal comfort and energy consumption.<sup>8</sup> An optimum synthesis of the films is critical for large scale implementation<sup>9</sup> since the methods of production must be low cost, efficient, and robust.<sup>10</sup> Several methods for synthesis are available, i.e., chemical vapor deposition,<sup>11</sup> sputtering, and others.<sup>12</sup> The chemical spray pyrolysis method<sup>13</sup> holds promise in the field of self-cleaning surfaces, but choosing a precursor solution is essential and determines the functionality of the system/film. Spiridonova *et al.* employed<sup>1</sup> titanium isopropoxide (TTIP) as a titanium precursor and acetylacetone (AcacH) as a stabilizing agent for the fabrication of TiO<sub>2</sub> films by ultrasonic spray pyrolysis (see the [supplementary material](#) for details on film preparation). For the TiO<sub>2</sub> films obtained from different TTIP to AcacH molar ratio, the photodegradation of stearic acid (SA) was monitored. It was shown that the reaction rate constant (k) increases by approximately an order of

magnitude with the increasing ratio. This was quantified by calculating the reaction rate constant of the SA via the photodegradation test, while varying the ratio of TiO<sub>2</sub> film synthesis from 1:1 (TTIP) to 1:8 (AcacH), where an optimum was found. The authors provided an interpretation for such improvement based on (1) a variation of morphology monitored via topographic AFM measurements, (2) wettability properties monitored by means of contact angle measurements, and (3) XPS measurements that showed a possible incorporation of carbon species on the surface of the TiO<sub>2</sub> film. In another recent study,<sup>14</sup> it was shown that increasing the amount of AcacH in the precursor solution promotes a transition from preferential fast electron to preferential fast hole transfer toward the TiO<sub>2</sub> surface, correlating with a strong increase in the photocatalytic decomposition rate of organic pollutants. Based on these studies, the possible mechanism for enhanced photocatalytic activity was related to passivation of electron traps at the surface, induced by incorporation of carbon impurities in TiO<sub>2</sub> films. Incorporating carbon impurities can induce “defect states” and related modifications to the band structure of the films, thus affecting the Fermi level locally.<sup>15</sup> For this reason, Kelvin Probe Force Microscopy (KPFM) can potentially provide information regarding

the changing/pinning of the Fermi level for the TiO<sub>2</sub> system investigated by Spiridonova *et al.*

Here, we characterize the surface of the TiO<sub>2</sub> films at different ratios with the AFM by means of KPFM.<sup>16</sup> The KPFM technique can be employed<sup>17</sup> to produce maps<sup>18</sup> of the contact potential difference (CPD) between the AFM tip and a sample's surface. In KPFM, the tip is grounded and the CPD is defined as  $CPD = (\phi_{tip} - \phi_s)/e$ , where  $\phi_s$  is the work function of the surface,  $\phi_{tip}$  is the work function of the tip, and  $e$  is the electron charge. The CPD can be identified with the necessary potential energy variations to the electron structure of the tip-sample system to produce a common Fermi level  $E_F$ .<sup>15</sup> The Fermi level is the work required to add an electron to a material,<sup>19</sup> while the work function is the minimum energy to remove an electron from it. This relationship is commonly written<sup>20</sup> in terms of the "vacuum" energy  $E_{VAC}$  as a reference as  $\phi = E_{VAC} - E_F$ , where the expression shows that the work function is simply the difference between the Fermi level and the vacuum level. While the Fermi alignment affects both tip and sample, only the Fermi level of the surface varies, i.e., the tip always remains the same during the experiment. Therefore, KPFM contrast maps, through the work function difference, provide information regarding the relative Fermi level/work function from sample to sample and from area to area on a sample's surface. Since the energy required to remove/add an electron can be provided by photon adsorption, these maps can be employed to interpret variations in photodegradation/photoreactivity. Thus, variations in CPD can be employed to discuss changes in the band structure. If photodegradation is related to Fermi level variations from sample to sample, variations in CPD should also be observed in the maps as a function of the TTIP to AcacH ratio, i.e., some form of correlation between CPD and photodegradation should be possible.

The synthesis of TiO<sub>2</sub> films, particularly in the case of the application under consideration, requires that contaminants, or pollutants, deposited on the TiO<sub>2</sub> surface degrade. The general principle in photodegradation is that the interaction of light with matter degrades pollutants<sup>21</sup> where reactive oxygen species (ROS)<sup>22,23</sup> have an important mediating role<sup>24</sup> in degradation. In the case of the TiO<sub>2</sub> films, and in real applications, pollutants are spontaneously deposited onto the TiO<sub>2</sub> surface from the environment. Here, emphasis is put in ROS, a collective term, rather than in free radicals alone, i.e., any species that

contains one or more unpaired electrons,<sup>22</sup> because a variety of radical and nonradical oxidizing species might be produced by photoreaction on the TiO<sub>2</sub> surface. In short, contaminants, from here forth more restrictively referred to as volatile organic compounds (VOCs), adsorb onto TiO<sub>2</sub> films and these degrade by the action of a set of ROS. An investigation of the presence, or absence thereof, of specific VOCs and ROS, as well as the possibility to quantify their concentration, would be a study worth carrying out, but the authors purposefully leave this question open and out of the current investigation. The aim is to focus on what can be learnt from the KPFM CPD maps alone for the different ratios and their relation to photodegradation functionality. Still, for the sake of discussion, a hypothetical and generic mechanism is illustrated in Fig. 1 and detailed with the help of Eqs. (1) and (2) in the following paragraphs. This cartoon is meant to show the role of light to activate the complex reactions in the process of photodegradation. The degradation process can be divided into three steps.<sup>23</sup>

In the first step, H<sub>2</sub>O in the proximity of the surface or weakly adsorbed H<sub>2</sub>O molecules and TiO<sub>2</sub> interact with photons of energy  $hf$  to produce ROS [Eq. (1) and Figs. 1(a) and 1(b)]. In Eqs. (1) and (2), *ad* means adsorbed. It is this light-matter interaction that is critical when it comes to degradation since it activates the whole process. While the mechanisms are complex, it is variations in the TTIP to AcacH ratio that should control this light-matter interaction and should be visible in terms of CPD values. No attempt is made here to fully elucidate this process chemically, and the double arrows in the reaction equations emphasize this point and point to the possible presence of intermediates. The reaction kinetics of such systems can be extremely complex to quantify and monitor, and many reactive species are possible.<sup>23</sup> A typical example of reactive species for this system with a lifespan in the range of femtoseconds is hydroxyl OH. (Chen *et al.* provide a rather comprehensive list of main reactions and reactive species.) In terms of photodegradation, the relevance is to be found in the final products, i.e., ROS, rather than in any intermediates while the production of these ROS is dependent on band structure and surface chemistry.

In the second step, the highly reactive agents (ROS) induce a set of reactions that lead to the degradation of VOCs ultimately resulting in the production of gases, such as CO<sub>2</sub> [Eq. (2) and Fig. 1(c)]. This stage is relevant both from a point of view of applied surface science

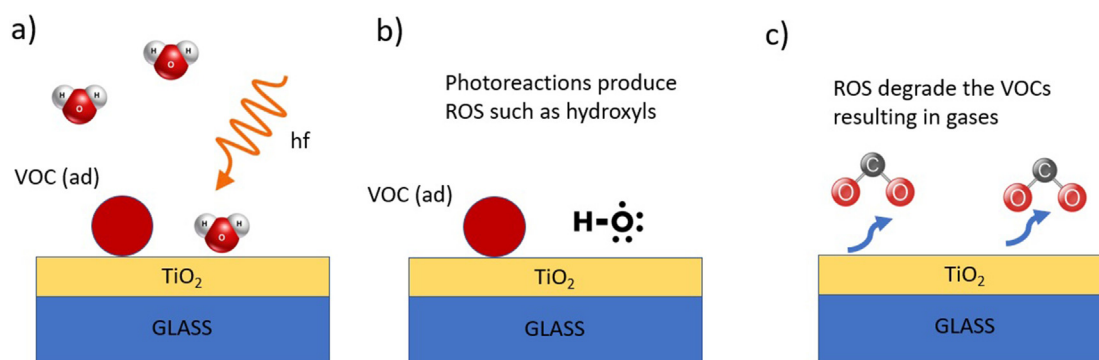


**FIG. 1.** Three step illustration of a possible mechanism for photodegradation, where ROS act as the degrading species. (a) Water molecules in the proximity of the surface, or weakly adhered (ad) to the surface, react with electrons emitted from the TiO<sub>2</sub> surface which have been excited by light. (b) ROS are produced and interact with VOCs. (c) The degradation of VOCs results in gases.

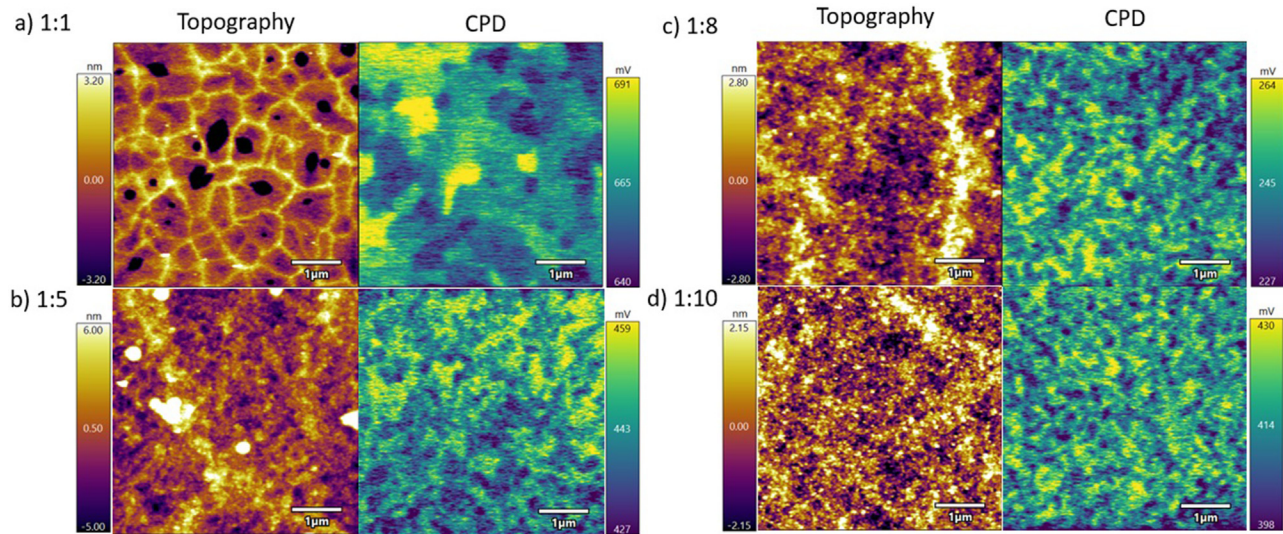


FIG. 2. Topography (left) and CPD (right) maps for the (a) 1:1, (b) 1:5, (c) 1:8, and (d) 1:10 ratios.

and theoretically, but it is also outside the scope of this work to elucidate it,



Standard KPFM was performed using the lift mode whereby a topography image was acquired first and then the cantilever was lifted to track the topography and cancel the voltage resulting from the work function difference. In the experiments, we used an MFP-3D AFM from Asylum Research. The probe was a HQ:NSC18/PT (Platinum coated) with resonant frequency  $\sim 75$  kHz and spring constant  $\sim 2$  N/m. The AFM was operated in the attractive regime in the amplitude modulation (AM) AFM mode. The lift height was set to 10 nm. The tip voltage was set to 1 V, and the electrical pass drive voltage was 3 V. Topography and corresponding CPD maps are shown in Fig. 2 for the ratios (a) 1:1, (b) 1:5, and (c) 1:8 and 1:10. Data for the 1:20 ratio were also collected, but the maps are not shown. Visual inspection alone shows that topography is not correlated with the CPD maps. Spiridonova *et al.* carried out photodegradation experiments by varying the TTIP to AcAcH ratio and exposing the samples to visible and UVA light (see the supplementary material for details on the lamp specifications). We also conducted the experiments by exposing the samples to visible light and UVA light (not all data shown). The samples were exposed for 20 min to UVA light before taking the data. An example of topography and CPD maps under (a) and (b) visible and (c) and (d) UVA light is shown in Fig. 3 for the (a) and (c) 1:1 and (b) and (d) 1:8 ratios.

The full data set for the experiments that we carried out is shown in Fig. 4 as histograms for the (a) UVA and (b) visible light experiments. Spiridonova *et al.* further reported higher photodegradation functionality when the samples were exposed to UVA, as opposed to exposure to visible light only, by monitoring and quantifying the photodegradation rate constants  $k$  ( $\text{min}^{-1}$ ). Their data are reproduced in Fig. 5 (red markers) against the results presented in Fig. 4 in terms of CPD (blue markers). The data have been normalized for convenience,

and all values used to produce Fig. 5 are shown in Tables I–IV. Since the rate constant  $k$  increases with decreasing CPD, the 1-normalized CPD values are plotted against normalized  $k$  in the figure. To normalize Fig. 5(a), the values are:  $k$  (minimum) =  $0.0016 \text{ min}^{-1}$ ,  $k$  (range) =  $0.0307 \text{ min}^{-1}$ ,  $V_{\text{CPD}}$  (minimum) = 249 mV, and  $V_{\text{CPD}}$  (range) = 764 mV. To normalize Fig. 5(b), the values are:  $k$  (minimum) =  $0.004 \text{ min}^{-1}$ ,  $k$  (range) =  $0.239 \text{ min}^{-1}$ ,  $V_{\text{CPD}}$  (minimum) = 213 mV, and  $V_{\text{CPD}}$  (range) = 710 mV. These values can be directly obtained from the respective tables (Tables I–IV). The mean values and

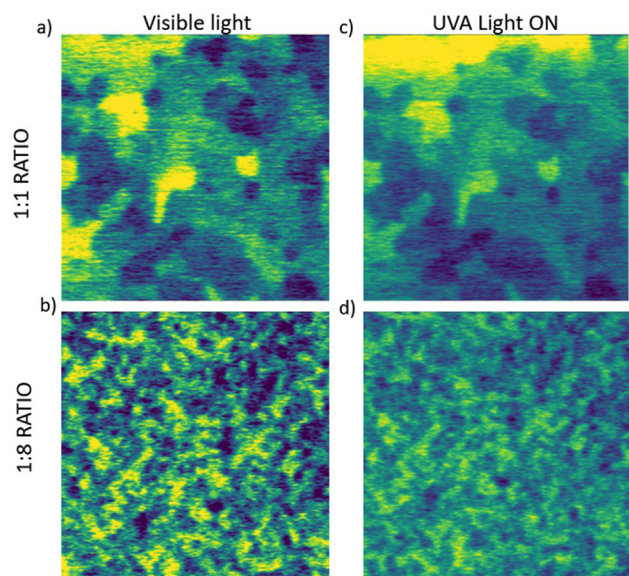
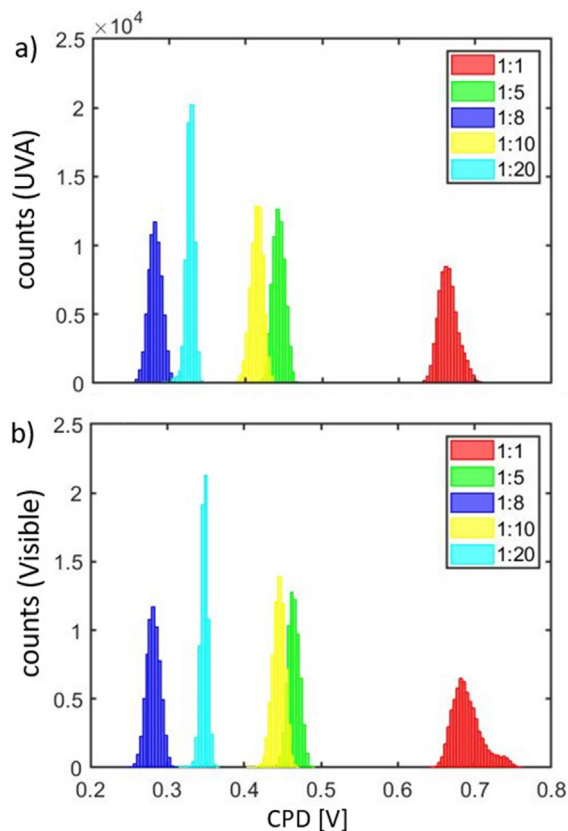


FIG. 3. CPD maps as the samples are exposed to visible light (a) and (b) and UVA (c) and (d) for the 1:1 and 1:8 ratios.



**FIG. 4.** Histograms showing the CPD data obtained in the KPFM experiments for (a) UVA exposed samples and (b) samples exposed to visible light. The data correspond to the  $512 \times 512$  pixels (262 144 points) obtained from contrast maps, i.e., those in Figs. 2 and 3.

standard deviations are shown in the figures. The key points to interpret Figs. 4 and 5 follow.

- (1) First, there is a shift in CPD in all cases toward lower CPD when the samples are exposed to UVA (compare the data in Table I with that in Table II where the data are presented for all samples in terms of the mean, standard deviation, range, minima, and maxima values);
- (2) Second, most importantly, the minimum values of CPD are always found for the ratio 1:8. The implication is that KPFM maps can be employed to identify photodegradation efficiency directly from CPD values.
- (3) Third, the maximum values of CPD are found for the ratio 1:1. It is known<sup>25</sup> that the ratio 1:1 is the least efficient, i.e., minimum  $k$  values. This was later confirmed by Spiridonova *et al.* that found the highest values at 1:8.
- (4) Fourth, the shift in CPD between exposing the samples to visible or UVA light is of approximately 20–40 mV for all ratios (Fig. 4). This shift is significant since the resolution of standard KPFM measurements is typically lower than 1 mV.<sup>17,26</sup>

The absolute value for the work function of the tip,  $\phi_{\text{tip}}$ , can be found by acquiring KPFM data from a calibration sample, such

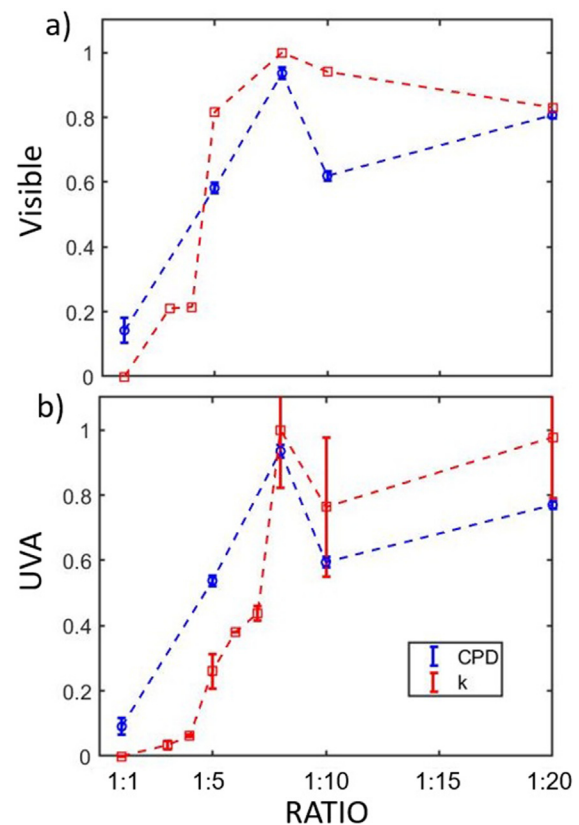


**FIG. 5.** Normalized CPD (blue markers) and  $k$  (red markers) values for the case where (a) the samples are exposed to (a) visible and (b) UVA light. Since  $k$  typically increases with CPD, the normalization for the CPD data is carried out as 1-CPD. The figures can be reproduced from the data provided in Tables I–IV.

as HOPG ( $\phi_{\text{HOPG}} \approx 4.6$  eV).<sup>27,28</sup> This calibration results in  $\phi_{\text{tip}} \approx 5.1$  eV. With this measurement, the absolute values for the different ratios can be obtained, i.e.,  $\phi_S \approx 4.4$  eV (ratio 1:1),  $\phi_S \approx 4.6$  eV (ratio 1:5),  $\phi_S \approx 4.8$  eV (ratio 1:8),  $\phi_S \approx 4.7$  eV (ratio 1:10), and  $\phi_S \approx 4.8$  eV (ratio 1:20). Lower CPD values correspond to higher values of work function for the samples. Thus, lower work functions for the TiO<sub>2</sub> films correlate with higher photodegradation efficiencies. This means that lower Fermi levels are obtained when the highest functionality is seen. It is known<sup>29</sup> that semiconductor p-doping, i.e., the production of holes or acceptors near the valence band, leads to lower Fermi levels while n-doping,

**TABLE I.** CPD measurements for the case when the samples are exposed to visible light.

TTIP:AcAcH	CPD (V)	Range	SD	Min. value	Max. value
1:1	0.691	0.120	0.020	0.644	0.764
1:5	0.464	0.068	0.008	0.424	0.492
1:8	0.282	0.063	0.009	0.249	0.311
1:10	0.445	0.066	0.008	0.405	0.471
1:20	0.348	0.047	0.005	0.320	0.367

**TABLE II.** CPD measurements for the case when the samples are exposed to UVA.

TTIP:AcacH	CPD (V)	Range	SD	Min. value	Max. value
1:1	0.665	0.085	0.013	0.625	0.710
1:5	0.443	0.061	0.008	0.409	0.471
1:8	0.246	0.061	0.009	0.213	0.274
1:10	0.415	0.087	0.008	0.358	0.446
1:20	0.328	0.064	0.006	0.283	0.347

**TABLE III.** Photodegradation rate constants under visible light.

TTIP:AcacH	k (min <sup>-1</sup> )	SD
1:1	0.001 63	0.000 17
1:3	0.008 05	0.001 46
1:4	0.008 19	0.001 59
1:5	0.026 67	0.003 81
1:8	0.032 33	0.005 90
1:10	0.030 52	0.010 53
1:20	0.027 11	0.002 17

**TABLE IV.** Photodegradation rate constants under UVA light.

TTIP:AcacH	k (min <sup>-1</sup> )	SD
1:1	0.003 98	...
1:3	0.012 02	0.002 83
1:4	0.018 76	0.000 87
1:5	0.066 22	0.012 50
1:6	0.094 71	0.000 06
1:7	0.108 53	0.005 64
1:8	0.242 73	0.042 48
1:10	0.186 22	0.051 03
1:20	0.237 43	0.045 00

i.e., the production of donors near the conduction band, leads to higher Fermi levels. A hypothesis can, thus, be brought forth whereby the lower Fermi levels are the result of hole creation, i.e., analogue to p-type doping, near the surface of the samples with highest photodegradation performance. Thus, the CPD signals obtained in our experiments might indicate the presence of faster transfer of charge carriers to the surface due to the presence of acceptors for the highest ratios. This interpretation is in good agreement with the trend in Surface PhotoVoltage Spectroscopy (SPV) signal discussed by Dittrich *et al.*<sup>14</sup> Fast transfer to the surface is beneficial for enhanced photocatalytic activity.

In summary, the above four points, together with the significant agreement in trends shown between k and CPD (Fig. 5) as a function of variations of the TTIP to AcacH molar ratio, show that the CPD and, therefore, the Fermi level of the samples control the photodegradation of the TiO<sub>2</sub> films. Clearly, while there is correlation between the

CPD values and the k values, the mechanisms involved in the overall process of photodegradation are complex and remain to be elucidated. It is possible that the carbon incorporation hypothesis leads to the lower Fermi levels observed whereby photodegradation is highest, i.e., highest TTIP to AcacH ratios. In analogy to p-type doping, lower Fermi levels hint at the presence of acceptors, i.e., holes, near the surface. The presence of these acceptors makes possible a faster transfer of charge carriers to the surface. Finally, since obtaining CPD data are relatively straightforward in KPFM, these results further provide the means to rapidly characterize the surfaces for photodegradation.

See the [supplementary material](#) for details on the synthesis of TiO<sub>2</sub> thin films and the specifications of UVA and visible light lamps used to monitor stearic acid degradation.

This study was funded by the Estonian Research Council project PRG627 “Antimony chalcogenide thin films for next-generation semi-transparent solar cells applicable in electricity producing windows,” the Estonian Centre of Excellence project TK141 (No. TAR16016EK) “Advanced materials and high-technology devices for energy recuperation systems,” and the European Union’s Horizon2020 programme under the ERA Chair project 5GSOLAR Grant Agreement No. 952509. This work was supported by ERDF project Centre of Technologies and Investigations of Nanomaterials (NAMUR+, Project No. 2014-2020.4.01.16-0123).

## AUTHOR DECLARATIONS

### Conflict of Interest

The authors have no conflicts to disclose.

### Author Contributions

**Tuza A Olukan:** Conceptualization (equal); Data curation (equal); Formal analysis (equal); Investigation (equal); Methodology (equal); Visualization (equal); Writing – original draft (equal); Writing – review and editing (equal). **Jekaterina Sydorenko:** Conceptualization (equal); Data curation (equal); Formal analysis (equal); Investigation (equal); Methodology (equal); Validation (equal); Visualization (equal); Writing – review and editing (equal). **Atanas Katerski:** Data curation (equal); Methodology (equal); Resources (equal); Validation (equal). **Mariam Al Mahri:** Conceptualization (equal); Investigation (equal); Visualization (equal). **Chia-Yun Lai:** Conceptualization (equal); Data curation (equal); Formal analysis (equal); Investigation (equal); Methodology (equal); Visualization (equal). **Abdulrahman Al-Hagri:** Conceptualization (equal); Investigation (equal); Methodology (equal); Validation (equal); Writing – original draft (equal); Writing – review and editing (equal). **Sergio Santos:** Conceptualization (equal); Formal analysis (equal); Investigation (equal); Methodology (equal); Project administration (equal); Resources (equal); Software (equal); Supervision (equal); Validation (equal); Visualization (equal); Writing – original draft (equal); Writing – review and editing (equal). **Matteo Chiesa:** Conceptualization (equal); Funding acquisition (lead); Investigation (supporting); Methodology (equal); Project administration (lead); Resources (lead); Supervision (lead); Writing – original draft (equal); Writing – review and editing (equal).

## DATA AVAILABILITY

The data that support the findings of this study are available within the article.

## REFERENCES

- <sup>1</sup>J. Spiridonova, A. Katerski, M. Danilson, M. Krichevskaya, M. Krunks, and I. O. Acik, *Molecules* **24**, 4326 (2019).
- <sup>2</sup>S. Banerjee, D. D. Dionysiou, and S. C. Pillai, *Appl. Catal. B* **176–177**, 396–428 (2015).
- <sup>3</sup>Y. Yang, Q. Lai, S. Mahmud, J. Lu, G. Zhang, Z. Huang, Q. Wu, Q. Zeng, Y. Huang, H. Lei, and Z. Xiong, *J. Membr. Sci.* **645**, 120204 (2022).
- <sup>4</sup>J. Schneider, M. Matsuoka, M. Takeuchi, J. Zhang, Y. Horiuchi, M. Anpo, and D. W. Bahnemann, *Chem. Rev.* **114**, 9919–9986 (2014).
- <sup>5</sup>M. J. Torralvo, J. Sanz, I. Sobrados, J. Soria, C. Garlisi, G. Palmisano, S. Çetinkaya, S. Yurdakal, and V. Augugliaro, *Appl. Catal. B* **221**, 140–151 (2018).
- <sup>6</sup>C. Garlisi, G. Scandura, G. Palmisano, M. Chiesa, and C. Y. Lai, *Langmuir* **32**, 11813–11818 (2016).
- <sup>7</sup>A. Mavrikos, D. Papoulis, N. Todorova, I. Papailias, C. Trapalis, D. Panagiotaras, D. A. Chalkias, E. Stathatos, E. Gianni, K. Somalakidi, D. Sygkridou, and S. Komarneni, *J. Photochem. Photobiol. A* **423**, 113568 (2022).
- <sup>8</sup>P. Chanklom, T. Kreetachat, R. Chotigawin, and K. Suwannahong, *ACS Omega* **6**, 10629–10636 (2021).
- <sup>9</sup>K. U. Ambikakumari Sanalkumar and E.-H. Yang, *Cem. Concr. Compos.* **115**, 103847 (2021).
- <sup>10</sup>T. Adachi, S. S. Latthe, S. W. Gosavi, N. Roy, N. Suzuki, H. Ikari, K. Kato, K. Katsumata, K. Nakata, M. Furudate, T. Inoue, T. Kondo, M. Yuasa, A. Fujishima, and C. Terashima, *Appl. Surf. Sci.* **458**, 917–923 (2018).
- <sup>11</sup>R. Mauchauffé, S. Kang, J. Kim, J.-H. Kim, and S. Y. Moon, *Curr. Appl. Phys.* **19**, 1296–1304 (2019).
- <sup>12</sup>B. Wei, J. L. Xue, H. T. Cao, H. G. Li, F. Wen, and Y. T. Pei, *Surf. Rev. Lett.* **26**, 1950036 (2019).
- <sup>13</sup>A. Juma, I. Oja Acik, A. T. Oluwabi, A. Mere, V. Mikli, M. Danilson, and M. Krunks, *Appl. Surf. Sci.* **387**, 539–545 (2016).
- <sup>14</sup>T. Dittrich, J. Sydorenko, N. Spalatu, N. H. Nickel, A. Mere, M. Krunks, and I. O. Acik, *ACS Appl. Mater. Interfaces* (2022) (unpublished).
- <sup>15</sup>P. A. Markeev, E. Najafidehaghani, Z. Gan, K. Sotthewes, A. George, A. Turchanin, and M. P. de Jong, *J. Phys. Chem. C* **125**, 13551–13559 (2021).
- <sup>16</sup>Y. Adachi, Y. Sugawara, and Y. J. Li, *Nano Res.* **15**, 1909–1915 (2022).
- <sup>17</sup>W. Melitz, J. Shen, A. C. Kummel, and S. Lee, *Surf. Sci. Rep.* **66**, 1–27 (2011).
- <sup>18</sup>C. Maragliano, S. Lilliu, M. S. Dahlem, M. Chiesa, T. Souier, and M. Stefancich, *Sci. Rep.* **4**, 4203 (2015).
- <sup>19</sup>N. W. Ashcroft and D. N. Mermin, *Solid State Physics* (Cengage Learning, 1976).
- <sup>20</sup>A. Kahn, *Mater. Horiz.* **3**, 7–10 (2016).
- <sup>21</sup>H. D. Burrows, M. Canle L, J. A. Santaballa, and S. Steenken, *J. Photochem. Photobiol. B* **67**, 71–108 (2002).
- <sup>22</sup>H. Bayr, *Crit. Care Med.* **33**, S498–S501 (2005).
- <sup>23</sup>B. Chen, C. Zhu, J. Fei, Y. Jiang, C. Yin, W. Su, X. He, Y. Li, Q. Chen, Q. Ren, and Y. Chen, *J. Hazard. Mater.* **363**, 55–63 (2019).
- <sup>24</sup>C. Challier, S. Laurella, P. Allegretti, C. Sabini, L. Sabini, N. A. García, A. Biasutti, and S. Criado, *Photochem. Photobiol.* **94**, 1151–1158 (2018).
- <sup>25</sup>A. O. Juma, I. O. Acik, V. Mikli, A. Mere, and M. Krunks, *Thin Solid Films* **594**, 287–292 (2015).
- <sup>26</sup>U. Zerweck, C. Loppacher, T. Otto, S. Grafström, and L. M. Eng, *Phys. Rev. B* **71**, 125424 (2005).
- <sup>27</sup>W. Melitz, J. Shen, S. Lee, J. S. Lee, A. C. Kummel, R. Droopad, and E. T. Yu, *J. Appl. Phys.* **108**, 023711 (2010).
- <sup>28</sup>Y. Lv, J. Cui, Z. M. Jiang, and X. Yang, *Nanoscale Res. Lett.* **7**, 659–659 (2012).
- <sup>29</sup>S. M. Sze and K. N. Kwok, *Physics of Semiconductor Devices* (Wiley Interscience, 2007).